

A Coupled BEM-MLPG Technique for the Thermal Analysis of Non-Homogeneous Media

A. Tadeu¹, P. Stanak², J. Sladek², V. Sladek², J. Prata¹, N. Simões¹

Abstract: This paper presents a technique that couples the boundary element method (BEM) with the meshless local Petrov-Galerkin (MLPG) method, formulated in the frequency domain. It is then used to study the transient heat diffusion through a two-dimensional unbounded medium containing confined subdomains where the material properties vary from point to point.

To exploit the advantages of each method, the BEM is used for the homogeneous unbounded domain and the MLPG method is used for the non-homogeneous confined subdomains. The nodal points placed at the interface between the confined subdomains and the unbounded homogenous medium are used to couple the BEM and the MPLG method. The MLPG method is formulated using the moving least-squares (MLS) approximation as the trial function and the Heaviside step function as the test function in local integral equations defined over small local sub-domains. The coupled BEM-MLPG approach is verified against the results provided by an analytical solution developed for a circular confined subdomain, in which the thermal diffusivity within the circular non-homogeneous region is assumed to vary in the radial direction. The proposed model is finally used to solve the case of a pair of non-homogeneous confined subdomains for which analytical solutions are not known. The analysis of time domain temperature responses is presented, which illustrates the applicability of the model.

Keywords: Meshless method, boundary element method, direct coupling, heat diffusion, non-homogeneous domains.

1 Introduction

The study of heat transfer is increasingly important in many branches of engineering. Several tools are currently available for the analysis of transient heat diffusion,

¹ ITeCons, University of Coimbra, Pólo II, Rua Pedro Hispano, 3030-289, Coimbra, Portugal.

² Institute of Construction and Architecture, Slovak Academy of Sciences, 84503 Bratislava, Slovakia.

based on analytical formulations [Carslaw and Jaeger (1959)] or numerical methods, such as the finite difference method (FDM) [Ozisk (1994); Juncu (2008)], the finite element method (FEM) [Bathe (1976)], the finite volume method (FVM) [Cai, Mandel and McCormick (1991)] and the boundary element method (BEM) [Brebbia, Telles and Wrobel (1984); Ochiai (2001); Abreu, Canelas and Mansur (2013)]. The BEM is possibly one of the most suitable tools for the analysis of heat diffusion in homogenous unbounded media since the far field boundary conditions are automatically satisfied, and only the discontinuities or interfaces of the materials require discretization. However, the BEM can only be applied to more general geometries and media when the relevant fundamental solutions or Green's functions, required in the boundary integral equation, are known. But for those problems involving non-homogenous media, with variation of material thermal properties, the fundamental solution is generally unavailable in the closed form.

However, mesh-based methods such as FEM, FVM and FDM have become well established over the last few years and have been successfully applied to the numerical analysis of transient heat diffusion problems in large models with more complex shapes but finite dimensions. However, if the model to be analyzed is too complex, the mesh generation process that is characteristic for these methods becomes very time-consuming and requires considerable computational effort.

Therefore, in recent years, a different type of numerical method has been developed as an alternative to the well established mesh-based methods or BEM, known as meshless methods or element free methods.

These methods require neither domain nor boundary discretization and consequently no information on the connectivity between nodal points and elements is needed, which eliminates some of the mathematical complexity of mesh-based methods and provides accurate solutions at substantially lower computational cost. One of the advantages of meshless methods is their ability to efficiently treat problems with continuously non-homogeneous domains, since the unknown field quantities are approximated only in terms of nodes instead of finite elements, thus the continuous variation of material properties is maintained exactly. The same does not occur in case of mesh-based methods such as FEM, where the material properties are constant for each finite element leading to piecewise homogeneous material properties in the considered domain.

Authors have successfully used a range of meshless methods to simulate transient heat conduction problems, such as the method of fundamental solutions MFS [Fairweather and Karageorghis (1998); Fairweather, Karageorghis and Martin (2003); Smyrlis (2006)], the element-free Galerkin (EFG) method [Singh and Tanaka (2006); Zhang, Zhang and Zhang (2013)], the reproducing kernel particle (RKP) method [Cheng and Liew (2009)] and the meshless local Petrov-Galerkin (MLPG) method

[Atluri and Zhu (1998)].

Unlike some of the methods mentioned above, the MLPG method [Atluri and Zhu (1998); Atluri (2004)] is a truly meshless method since it does not need a background mesh for the numerical integration. It is based on the local weak form of governing equations over small subdomains specified for each nodal point. All integrals can be easily evaluated over these regularly shaped, overlapping subdomains of arbitrary shape (in general, circles for 2D problems and spheres for 3D problems) and their respective boundaries. There is only one nodal point in each subdomain, thus the local sense of the approach is kept. In the MLPG method trial and test functions can be chosen from different functional spaces, allowing for several various MLPG formulations [Atluri and Shen (2002)].

The MLPG has been successfully applied to different problems in engineering including elastostatics [Atluri, Sladek, Sladek and Zhu (2000); Sellountos, Vavourakis and Polyzos (2005); Vavourakis and Polyzos (2007); Sladek, Sladek and Zhang (2008)], elastodynamics [Sladek, Sladek and Van Keer (2003); Soares, Sladek and Sladek (2012)], plates and shells [Soric, Li, Jarak and Atluri (2004); Sladek, Sladek, Wen and Aliabadi (2006); Sladek Sladek and Sator (2013)], fracture problems [Ching and Batra (2001); Sladek, Sladek, Krivacek and Zhang (2005); Han, Liu, Rajendran and Atluri (2006)], fluid flow [Lin and Atluri (2001); Avila and Atluri (2009)], coupled multiphysics problems [Sladek et al. (2006); Shirzadi, Sladek and Sladek (2013)] and heat transfer [Sladek, Sladek and Atluri (2004); Wu and Tao (2008); Sladek, Sladek, Tanaka and Zhang (2005)]. The application of the MLPG method to a broad range of scientific problems is summarized in the review article by Sladek et al. (2013).

The MLPG method has been employed more often in steady-state and transient heat transfer problems in recent years. Solutions for transient heat conduction in functionally graded materials (FGMs) were also developed [Sladek, Sladek and Zhang (2003), Sladek, Sladek, Krivacek and Zhang. (2003); Sladek et al. (2005)] for axisymmetric [Sladek, Sladek, Hellmich and Eberhardsteiner (2007)] and 3D bodies [Sladek, Sladek, Tan and Atluri (2008)]. Wu and Tao (2008) used the MLPG method to compute 2D steady-state heat conduction problems involving irregular complex domains. MLPG and finite volume method (FVM) responses were compared, showing the good accuracy of the proposed model. Mirzaei and Dehghan (2011) proposed using the MLS approximation scheme in both the time and space domains to analyze transient heat conduction problems by MLPG method. Dai et al presented an improved MLPG method to calculate 2D unsteady-state heat conduction problems using the moving Kriging interpolation as the trial function and the Heaviside step function as the test function [Dai, Zheng, Liang and Wang (2013)]. The accuracy of the proposed model was evaluated considering the transient heat

conduction problem in a square and a rectangular domain and comparing the results with those obtained with analytical solutions and FEM. Li et al proposed a combined approach of the MLPG method based on the natural neighbor interpolation (NNI) and the modified precise time step integration method (MPTSIM) in the time domain to perform transient heat conduction analysis on square domains [Li, Chen and Kou (2011)]. Techapirom and Luadsong have used an MLPG method to study the two-dimensional heat equation with Dirichlet, Neumann and non-local boundary conditions in a square domain. Their study demonstrated the good accuracy of the proposed method and indicates that it can be easily extrapolated to other problems [Techapirom and Luadsong (2013)]. Inverse problems of heat conduction also attracted some attention. Sladek et al applied the MLPG to inverse heat conduction problems in 2D and 3D axisymmetric bodies [Sladek, Sladek and Hon (2006)]. MLPG solutions to inverse heat conduction problems in 3D anisotropic FGM solids [Sladek, Sladek, Wen and Hon (2012)] and inverse problems of determining the unknown heat conduction coefficients have also recently been presented [Sladek, Sladek, Wen and Hon (2009)].

However, like mesh-based techniques, the meshless methods have their own disadvantages and limitations. The interpolations and the algorithm implementation of meshless methods tend to be computationally expensive and for problems with infinite and semi-infinite domains these methods may be inefficient [Gu and Liu (2005)]. Furthermore, in meshless methods using moving least squares (MLS) shape functions, the essential boundary conditions can be very difficult to implement [Gu and Liu (2005)]. Therefore, many researchers have been proposing the mutual coupling of properly selected methods, in order to alleviate specific limitations of individual methods. The MLPG method coupled with FEM has been applied to problems involving elasticity factors [Liu and Gu, 2000], potential problems [Chen and Raju (2003)], electromagnetic field computations [Zhao and Nie (2008)], and to the fracture analysis of magneto-electro-elastic materials [Li, Feng and Xu (2009)]. Other examples include combining BEM with MFS [Tadeu, Simões and Simões (2010); Godinho, Tadeu and Simões (2006)], BEM with meshless Kansa's method [Godinho and Tadeu (2012)], FEM with EFG method [Belytschko, Organ and Krongauz (1995); Hegen (1996); Karutz, Chudoba and Kratzig (2002)], BEM with EFG method [Zan Zhang, Cheng (2008); Liu and Gu (2000)], Trefftz method and Voronoi cells [Dong and Atluri (2012)], and symmetric Galerkin BEM (SGBEM) with Voronoi cells for micromechanical analysis [Dong and Atluri (2013)], and so on. To improve the computational efficiency of weak formulations based on meshless approximations, analytical integrations have been proposed in elastostatics [Sladek and Sladek (2010)] and potential problems [Sladek, Sladek and Zhang (2010)], and they have also been successfully utilized

in elastodynamics [Soares, Sladek and Sladek (2012)].

In this work we propose a BEM and MLPG coupling, formulated in the frequency domain for the analysis of transient heat diffusion through an unbounded homogeneous domain containing inclusions with non-homogeneous variation of thermal properties. The thermal diffusivity inside the inclusion is assumed to vary in a smooth fashion. The advantages of each method are exploited using the BEM for the homogeneous unbounded domain and the MLPG for the non-homogeneous inclusion. Nodal points are introduced inside the non-homogeneous domain and on the interface, where the same nodal points are used for the specification of boundary elements. The continuity condition for the temperature and heat flux is specified at these interface nodes. The moving-least squares (MLS) approximation is applied in the MLPG formulation for the approximation of unknown nodal quantities inside the non-homogeneous domain, and for the continuity conditions. This direct coupling method does not require the iterative technique [Soares (2009)] or the concept of overlapping ‘double nodes’ for mutual BEM-MLPG coupling.

The proposed method is verified against an analytical solution known for a simple geometry [Tadeu, Prata and Simões (2012)]. Some conclusions are drawn and the quality of the numerical results is discussed.

In the paragraphs that follow, the problem is defined, and then the MLPG and BEM coupling formulations are established for heterogeneous domains embedded in an unbounded medium. The coupling formulations are verified against the responses obtained using analytical solutions. Finally, a numerical example is used to illustrate the applicability of the proposed method. The responses in the time domain are obtained by means of a fast inverse Fourier transform.

2 Problem definition

Consider a domain composed of two subdomains, $\Omega = \Omega_1 \cup \Omega_2$, with Ω_2 being unbounded and filled with a homogeneous medium, while in subdomain Ω_1 , the density, ρ_1 , the specific heat c_1 and the thermal conductivity λ_1 are assumed to vary from point to point (see Fig. 1). This system is excited by a heat point source located at $\mathbf{x}_0 = (x_0, y_0)$.

The transient heat transfer by conduction to calculate the temperature, $T(x, t)$, at a point (x, y) of the spatial 2D heterogeneous solid domain, Ω_1 is given by the diffusion equation in Cartesian coordinates:

$$\frac{\partial}{\partial x} \left(\lambda_1(\mathbf{x}) \frac{\partial T(\mathbf{x}, t)}{\partial x} \right) + \frac{\partial}{\partial y} \left(\lambda_1(\mathbf{x}) \frac{\partial T(\mathbf{x}, t)}{\partial y} \right) = \rho_1(\mathbf{x}) c_1(\mathbf{x}) \frac{\partial T(\mathbf{x}, t)}{\partial t} \quad (1)$$

in which t is time and $\mathbf{x} \equiv (x, y)$. The application of a Fourier transform in the time

domain leads to the following equation,

$$\frac{\partial}{\partial x} \left(\lambda_1(\mathbf{x}) \frac{\partial T(\mathbf{x}, \omega)}{\partial x} \right) + \frac{\partial}{\partial y} \left(\lambda_1(\mathbf{x}) \frac{\partial T(\mathbf{x}, \omega)}{\partial y} \right) - i\omega \frac{\lambda_1(\mathbf{x})}{K_1(\mathbf{x})} T(\mathbf{x}, \omega) = 0 \quad (2)$$

where $T(\mathbf{x}, \omega) = \int_0^\infty T(\mathbf{x}, t) e^{-i\omega t} dt$, ω is the frequency, and $K_1(\mathbf{x}) = \lambda_1(\mathbf{x}) / (\rho_1(\mathbf{x}) c_1(\mathbf{x}))$ is the thermal diffusivity. Recall that Eq. 2 is the PDE with variable coefficients, so BEM cannot be used.

In the unbounded domain Ω_2 , with constant thermal diffusivity $K_2 = \lambda_2 / (\rho_2 c_2)$, Eq. 1 can be transformed into the following equation:

$$\left(\frac{\partial^2}{\partial x^2} + \frac{\partial^2}{\partial y^2} + (k_{c2})^2 \right) T(\mathbf{x}, \omega) = 0, \quad k_{c2} = \sqrt{\frac{-i\omega}{K_2}} \quad (3)$$

which is the PDE with constant coefficients.

In the frequency domain, the incident temperature field, T_{inc} generated at a point (x, y) by a source placed in Ω_2 at a point (x_0, y_0) is given by:

$$T_{inc}(x, y, \omega) = \frac{-iA}{4\lambda_2} H_0^{(2)} \left(K_2 \sqrt{(x - x_0)^2 + (y - y_0)^2} \right) \quad (4)$$

where $H_0^{(2)}(\dots)$ is the Hankel function of the second kind and order 0.

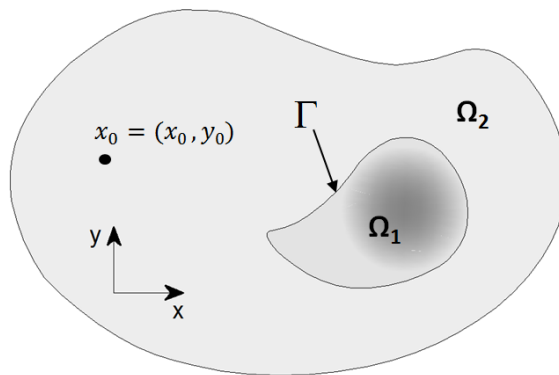


Figure 1: Problem definition

The problem is solved using the MLPG method to model the heterogeneous medium, and the BEM to model the unbounded homogeneous medium. This approach overcomes the limitations of each method. The coupling between the two methods is accomplished by imposing the continuity of temperatures and heat fluxes across the boundary of the heterogeneous subdomain.

2.1 Meshless Local Petrov-Galerkin (MLPG) formulation

In the MLPG method trial and test functions can be chosen from different functional spaces, allowing for several various MLPG formulations. In the proposed approach, the MLPG5 method is chosen assuming MLS approximation to represent the trial functions and Heaviside unit step function as a test function in each local subdomain Ω_S , as shown in Fig. 2. Instead of writing the global weak form, the MLPG is based on the local weak form of governing equations. The local weak form of Eq. 2 is then written over each subdomain Ω_S as

$$\int_{\Omega_S} (\lambda_1(\mathbf{x})T_{,j}(\mathbf{x}, \omega))_{,j} w^*(\mathbf{x})d\Omega - i\omega \int_{\Omega_S} \frac{\lambda_1(x)}{K_1(x)} T(\mathbf{x}, \omega)w^*(\mathbf{x})d\Omega = 0 \tag{5}$$

in which $\mathbf{x} \equiv (x, y)$.

Applying the Gauss divergence theorem for the first integral in (2) leads to

$$\int_{\partial\Omega_S} \lambda_1(\mathbf{x}) \mathbf{n}(\mathbf{x}) \cdot \nabla T(\mathbf{x}, \omega) w^*(\mathbf{x})d\partial\Omega - \int_{\Omega_S} \lambda_1(\mathbf{x}) \nabla T(\mathbf{x}, \omega) \cdot \nabla w^*(\mathbf{x}) d\Omega - i\omega \int_{\Omega_S} \frac{\lambda_1(\mathbf{x})}{K_1(\mathbf{x})} T(\mathbf{x}, \omega) w^*(\mathbf{x}) d\Omega = 0 \tag{6}$$

where $n_k(\mathbf{x})$ is the unit normal vector and $\partial\Omega_S$ is the boundary of the subdomain Ω_S . Assuming the Heaviside unit step function for the test function

$$w^*(\mathbf{x}) = \begin{cases} 1 & \text{at } \mathbf{x} \in (\Omega_S \cup \partial\Omega_S) \\ 0 & \text{at } \mathbf{x} \notin (\Omega_S \cup \partial\Omega_S) \end{cases} \tag{7}$$

the following local integral equation

$$\int_{\partial\Omega_S} \lambda_1(\mathbf{x}) \frac{\partial T(\mathbf{x}, \omega)}{\partial \mathbf{n}} d\partial\Omega - i\omega \int_{\Omega_S} \frac{\lambda_1(x)}{K_1(x)} T(\mathbf{x}, \omega)d\Omega = 0 \tag{8}$$

is finally obtained.

2.1.1 Numerical implementation of the MLPG method

The MLPG method is formulated using the moving least-squares (MLS) to approximate the temperature field over a number of nodal points randomly distributed over domain 1 and the interface with domain 2, by using a set of nodes across the domain of influence. According to the MLS method [Atluri (2004)], the approximation of the temperature field $T(\mathbf{x})$ over a number of randomly located nodes $\{\mathbf{x}^i\}$, $i = 1, 2, \dots, N$, is given by the following equation:

$$T(\mathbf{x}) = \boldsymbol{\pi}^T(\mathbf{x})\mathbf{a}(\mathbf{x}) \tag{9}$$

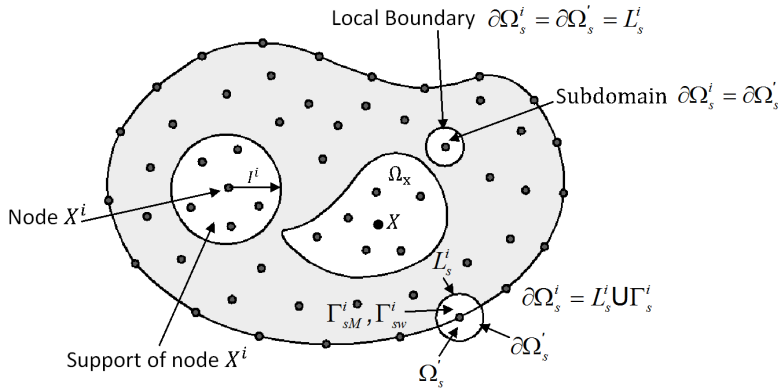


Figure 2: Local boundaries for weak formulation, the domain Ω_x for MLS approximation of the trial function, and support area of weight function around node

where $\boldsymbol{\pi}^T(\mathbf{x}) = [\pi^1(\mathbf{x}), \pi^2(\mathbf{x}), \dots, \pi^m(\mathbf{x})]$ is a complete monomial basis of order m ; and $\mathbf{a}(\mathbf{x}, \boldsymbol{\tau})$ is a vector containing the coefficients $a^j(\mathbf{x}, \boldsymbol{\tau})$, $j = 1, 2, \dots, m$ and $\mathbf{x} \equiv (x, y)$. For a 2D problem, monomial bases are expressed by the coordinates (x, y) and can be chosen as

$$\text{Linear basis: } \boldsymbol{\pi}^T(\mathbf{x}) = [1, x, y], \quad m = 3 \tag{10}$$

$$\text{Quadratic basis: } \boldsymbol{\pi}^T(\mathbf{x}) = [1, x, y, x^2, xy, y^2], \quad m = 6 \tag{11}$$

The coefficient vector $\mathbf{a}(\mathbf{x})$ is determined by minimizing a weighted discrete L_2 -norm defined as

$$J(\mathbf{x}) = \sum_{i=1}^N w^i(\mathbf{x}) [\boldsymbol{\pi}^T(\mathbf{x}^i)\mathbf{a}(\mathbf{x}) - \hat{T}^i]^2 \tag{12}$$

where N is the number of nodes used for the approximation. It is determined by the weight function $w^i(\mathbf{x})$ associated with the node i . Symbols \hat{T}^i are the fictitious nodal values, but not the nodal values of the unknown trial function in general. A 4th order spline-type weight function is then applied in the form

$$w^i(\mathbf{x}) = \begin{cases} 1 - 6 \left(\frac{d^i}{r^i}\right)^2 + 8 \left(\frac{d^i}{r^i}\right)^3 - 3 \left(\frac{d^i}{r^i}\right)^4 & 0 \leq d^i \leq r^i \\ 0 & d^i \geq r^i \end{cases} \tag{13}$$

where $d^i = \|\mathbf{x} - \mathbf{x}^i\|$ and r^i is the radius of the circular support domain. With Eq. 13, the C^1 -continuity of the weight function is ensured over the entire domain.

The regularity of the matrix \mathbf{A} is ensured by having the size of the support r^i cover a sufficient number of nodes in the domain of definition. The number of nodes lying in the support domain with radius r^i determines the value of N . Thus at least $N = m + 1$ nodes are required to fall into the support domain.

The stationarity of J in Eq. 12 with respect to $\mathbf{a}(\mathbf{x})$ leads to the following linear relation between $\mathbf{a}(\mathbf{x})$ and \hat{T}

$$\mathbf{A}(\mathbf{x})\mathbf{a}(\mathbf{x}) - \mathbf{B}(\mathbf{x})\hat{T} = 0 \tag{14}$$

where

$$\mathbf{A}(\mathbf{x}) = \sum_{i=1}^N w^i(\mathbf{x})\boldsymbol{\pi}(\mathbf{x}^i)\boldsymbol{\pi}^T(\mathbf{x}^i) \tag{15}$$

$$\mathbf{B}(\mathbf{x}) = [w^1(\mathbf{x})\boldsymbol{\pi}(\mathbf{x}^1), w^2(\mathbf{x})\boldsymbol{\pi}(\mathbf{x}^2), \dots, w^N(\mathbf{x})\boldsymbol{\pi}(\mathbf{x}^N)]$$

The solution of Eq. 14 for $\mathbf{a}(\mathbf{x})$ and a subsequent substitution into Eq. 9 gives approximation formulas for the temperature field as

$$T(\mathbf{x}) = \sum_{i=1}^N \varphi^i(\mathbf{x})\hat{T}^i \tag{16}$$

Where

$$\varphi^i(\mathbf{x}) = \sum_{j=1}^m \boldsymbol{\pi}^j(\mathbf{x}) (\mathbf{A}^{-1}(\mathbf{x})\mathbf{B}(\mathbf{x}))^{ji} \tag{17}$$

The expression for $\varphi^i(\mathbf{x})$ is usually referred to as the shape function of the MLS approximation corresponding to the nodal point \mathbf{x}^i .

For the approximation of the normal derivative of temperature (heat flux) one can use

$$\frac{\partial T}{\partial \mathbf{n}}(\mathbf{x}) = \sum_{i=1}^N \frac{\partial}{\partial \mathbf{n}} \varphi^i(\mathbf{x})\hat{T}^i = \sum_{i=1}^N n_k \varphi_{,k}^i(\mathbf{x})\hat{T}^i \tag{18}$$

in which the shape function derivative is obtained as

$$\varphi_{,k}^i = \sum_{j=1}^m \left[\boldsymbol{\pi}_{,k}^j (\mathbf{A}^{-1}\mathbf{B})^{ji} + \boldsymbol{\pi}^j (\mathbf{A}^{-1}\mathbf{B}_{,k} + \mathbf{A}_{,k}^{-1}\mathbf{B})^{ji} \right] \tag{19}$$

where $\mathbf{A}_{,k}^{-1} = (\mathbf{A}^{-1})_{,k}$ represents the derivative of the inverse of \mathbf{A} with respect to x_k , which is given by $\mathbf{A}_{,k}^{-1} = -\mathbf{A}^{-1}\mathbf{A}_{,k}\mathbf{A}^{-1}$.

Inserting Eqs. 16, 18 into Eq. 8 leads to a discretized local integral equation (LIE) in the form

$$\sum_{i=1}^N \hat{T}^i \int_{\partial\Omega_s} \lambda_1(\mathbf{x}) n_k(\mathbf{x}) \phi_{,k}^i(\mathbf{x}) d\partial\Omega - i\omega \sum_{i=1}^N \hat{T}^i \int_{\Omega_s} \frac{\lambda_1(\mathbf{x})}{K_1(\mathbf{x})} \phi^i(\mathbf{x}) d\Omega = 0 \quad (20)$$

Eq. (20) is applied at all interior nodes \mathbf{x}^l , ($l = 1, 2, \dots, N_{in}$) located inside the domain Ω_1 with $\Omega_s^l \subset \Omega_1$. The BEM approach is used for the nodes on the boundary. Boundary elements having one node in the centre of the element are used. These nodes are also used for the MLS approximations (16), (18).

2.2 Boundary element method (BEM) formulation

The required integral equation over a boundary Γ for the analysis of Eq. 3 in the unbounded domain Ω_2 can be constructed by applying the reciprocity theorem, leading to:

$$aT(\mathbf{x}_0, \omega) = \int_{\Gamma} G(\mathbf{x}, \mathbf{x}_0) \left(\frac{\partial T}{\partial \mathbf{n}} \right)_2(\mathbf{x}, \omega) d\Gamma - \int_{\Gamma} H(\mathbf{x}, \mathbf{x}_0, \mathbf{n}) T(\mathbf{x}, \omega) d\Gamma + T_{inc}(\mathbf{x}_0, \mathbf{x}_f) \quad (21)$$

where a is a constant that takes the value 0.5 for a point over a smooth boundary and the value 1 for a point within the domain, $G(\mathbf{x}, \mathbf{x}_0)$, $H(\mathbf{x}, \mathbf{x}_0, \mathbf{n})$ are the Green's function for temperature and its normal derivative, respectively, $q_2 = -\lambda_2(\partial T / \partial \mathbf{n})_2$ represents the heat flux in the domain Ω_2 and $T_{inc}(\mathbf{x}_0, \mathbf{x}_f)$ represents the incident temperature field generated by a point load located within the domain at \mathbf{x}_f .

The required two-dimensional Green's functions for temperature and heat flux for the unbounded medium are respectively given by

$$G(\mathbf{x}, \mathbf{x}_0) = -\frac{i}{4\lambda_2} H_0^{(2)} \left(K_2 \sqrt{(x-x_0)^2 + (y-y_0)^2} \right) \quad (22)$$

$$H(\mathbf{x}, \mathbf{x}_0) = \frac{i}{4\lambda_2} K_2 H_1^{(2)} \left(K_2 \sqrt{(x-x_0)^2 + (y-y_0)^2} \right) \frac{\partial r}{\partial \eta_n} \quad (23)$$

where $H_0^{(2)}(\dots)$ is the Hankel function of the second kind and order 0.

The numerical solution of Eq. 21 by BEM involves discretizing the boundary Γ into a set of N_{be} boundary elements, leading to

$$aT(\mathbf{x}_0, \omega) = \sum_{j=1}^{N_{be}} \int_{\Gamma_j} G(\mathbf{x}, \mathbf{x}_0) \left(\frac{\partial T}{\partial \mathbf{n}} \right)_2(\mathbf{x}, \omega) d\Gamma_j - \sum_{j=1}^{N_{be}} \int_{\Gamma_j} H(\mathbf{x}, \mathbf{x}_0, \mathbf{n}) T(\mathbf{x}, \omega) d\Gamma_j + T_{inc}(\mathbf{x}_0, \mathbf{x}_f)$$

$$(24)$$

The integrations along the boundary element Γ_j can be evaluated using a Gaussian quadrature scheme when the element to be integrated is not the loaded element. However, for the loaded element (the singular element) the integrands exhibit a singularity and to ensure that the method is accurate the integration should be carried out in closed form [Tadeu, Prata and Simões (2012)].

2.3 BEM-MLPG coupling

The present approach exploits a direct coupling between the BEM and MLPG. This is applicable when the nodes used by the BEM match the nodes used by the MLPG (as shown in Fig. 3). If the boundary nodes coincide then the continuity of temperature and heat flux can be imposed. Then imposition of these continuity conditions on Eq. 24 can be specified as

$$\begin{aligned}
 aT(\mathbf{x}_0, \omega) = & \sum_{j=1}^{N_{be}} \int_{\Gamma_j} G(\mathbf{x}, \mathbf{x}_0) \frac{\lambda_1(\mathbf{x})}{\lambda_2} \left(\frac{\partial T}{\partial \mathbf{n}} \right)_1(\mathbf{x}, \omega) d\Gamma_j \\
 & - \sum_{j=1}^{N_{be}} \int_{\Gamma_j} H(\mathbf{x}, \mathbf{x}_0, \mathbf{n}) T(\mathbf{x}, \omega) d\Gamma_j + T_{inc}(\mathbf{x}_0, \mathbf{x}_f)
 \end{aligned}
 \tag{25}$$

Note that the following relationship defining the continuity of heat flux q_1 and q_2 has been adopted,

$$\left(\frac{\partial T}{\partial \mathbf{n}} \right)_2 = \frac{\lambda_1}{\lambda_2} \left(\frac{\partial T}{\partial \mathbf{n}} \right)_1
 \tag{26}$$

with \mathbf{n} being the outward unit normal vector on boundary elements of the domain Ω_2 .

Since both the boundary temperatures $T(\mathbf{x})$ and $(\partial T / \partial \mathbf{n})_1$ on each boundary element Γ_j can be expressed according to the approximations given by Eqs. 16 and 18 in terms of nodal unknowns \hat{T}^i , a direct coupling of BEM and MLPG is possible. Then, substituting the MLS approximations (16), (18) into the boundary integral Eq. 24, one obtains:

$$\begin{aligned}
 aT(\mathbf{x}_0) = & \sum_{j=1}^{N_{be}} \int_{\Gamma_j} G(\mathbf{x}, \mathbf{x}_0) \sum_{i=1}^N \frac{\lambda_1(\mathbf{x})}{\lambda_2} n_k(\mathbf{x}) \varphi_{,k}^i(\mathbf{x}) \hat{T}^i d\Gamma_j \\
 & - \left[\sum_{j=1}^{N_{be}} \int_{\Gamma_j} H(\mathbf{x}, \mathbf{x}_0, \mathbf{n}) \sum_{i=1}^N \varphi^i(\mathbf{x}) \hat{T}^i d\Gamma_j + a \sum_{i=1}^N \varphi^i(\mathbf{x}_0) \hat{T}^i \right] + T_{inc}(\mathbf{x}_0, \mathbf{x}_f)
 \end{aligned}$$

(27)

Taking Eq. 27 for the N_{be} nodes on the interface between the domains and Eq. 20 for the N_{bi} ($N_{bi} + N_{be} = N_{total}$) interior nodes is leading to a complete system of equations for the unknown complex coefficients \hat{T}^i .

After solving the system, the nodal values for temperatures and heat fluxes can be retrieved by inserting \hat{T}^i into Eqs. 16 and 18 and Eq.26, respectively.

3 Verification and accuracy of the proposed model

To verify and study the accuracy of the proposed model, consider a non-homogeneous circular region, Ω_1 , of radius 1.0 m, centered at $(x = 0.0 \text{ m}, y = 0.0 \text{ m})$, embedded in an unbounded medium, Ω_2 . This inclusion is subjected to an external heat point source, T_{inc} , located at a given point $(x_0 = -2.5 \text{ m}, y_0 = 0.0 \text{ m})$ of the outer domain.

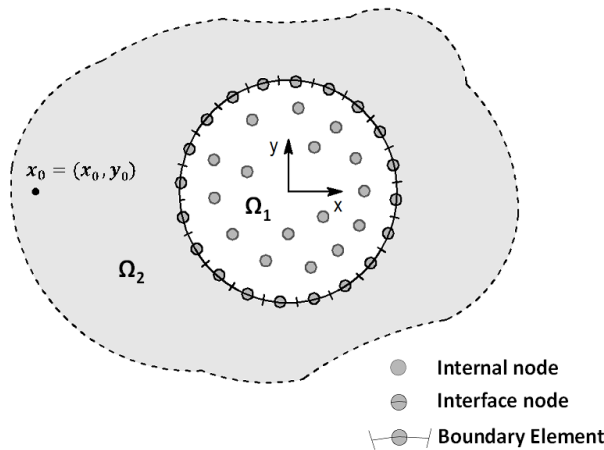


Figure 3: Geometry of the problem used for algorithm verification

The density, ρ , the specific heat c and the conductivity, λ of the outer medium are known ($\rho_2 = 1860 \text{ kg.m}^{-3}$, $c_2 = 780 \text{ J.kg}^{-1}.\text{°C}^{-1}$ and $\lambda_2 = 0.72 \text{ W.m}^{-1}.\text{°C}^{-1}$). The thermal properties c and λ within the circular non-homogeneous region are assumed to vary in the radial direction, according to the following relations:

$$\begin{aligned} \lambda_1(\mathbf{x}) &= 0.72 \left[1 + 1.5833 \left[1.0 + \sin \left(\pi \sqrt{x^2 + y^2} + \frac{\pi}{2} \right) \right] \right] \\ c_1(\mathbf{x}) &= 780 \left[1.25 - \frac{\sqrt{x^2 + y^2}}{4} \right] \\ \rho_1 &= 1860 \text{ kg.m}^{-3} \end{aligned} \tag{28}$$

for which an analytical solution can be obtained assuming a multilayered system defined by a sequence of concentric ring-shaped regions with different material properties [Tadeu, Prata and Simões (2012)]. The parameter ρ_1 has the same value as the external medium.

3.1 Verification and accuracy of the proposed model

Numerous tests were performed to understand the global behavior within the domain. The temperature field recorded at a grid of 6561 receivers, equally spaced 0.05 m apart in the two orthogonal directions and placed between ($x = -2.0$ m; $y = -2.0$ m) and ($x = 2.0$ m; $y = 2.0$ m), was computed.

The nodes' distribution within the circular non-homogeneous region is illustrated in Fig. 4. 100 boundary nodes and 701 internal nodes were considered.

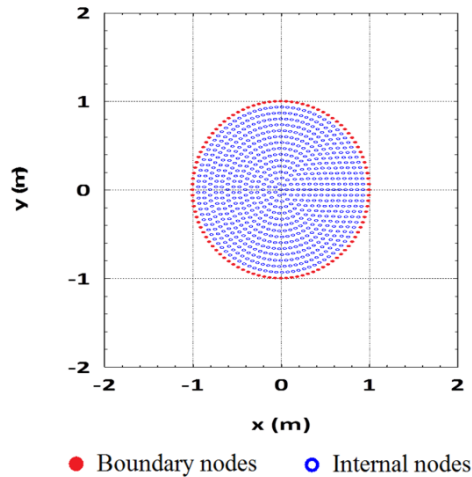


Figure 4: Node distribution for 100 boundary nodes and 701 internal nodes

Fig. 5 a) and Fig. 5 b) illustrate the conductivity and the specific heat variations, respectively.

Fig. 6 a) to 6 d) illustrate the responses obtained for frequency $5.0e^{-8}$ Hz. These figures show the real and imaginary parts of the analytical response and the numerical error obtained when the system is solved using the proposed model. It can be observed that the magnitude of the error increases the nearer the receivers are to the circular non-homogeneous region, and its value is higher at receivers nearest the heat source. However, analysis of these results shows that the numerical errors are small.

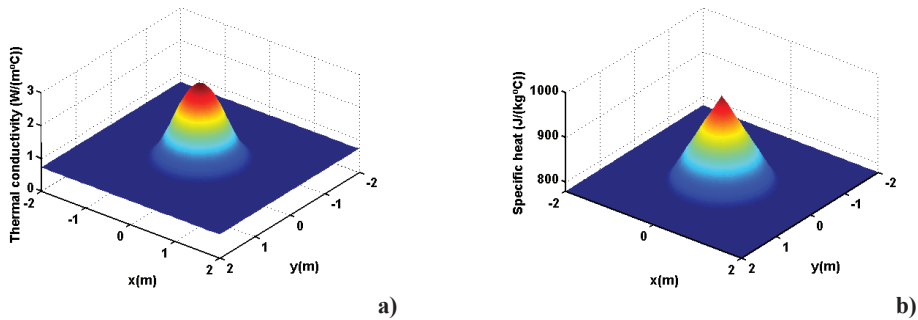


Figure 5: Variation of thermal properties for the test problem: a) Thermal conductivity distribution; b) Specific heat distribution

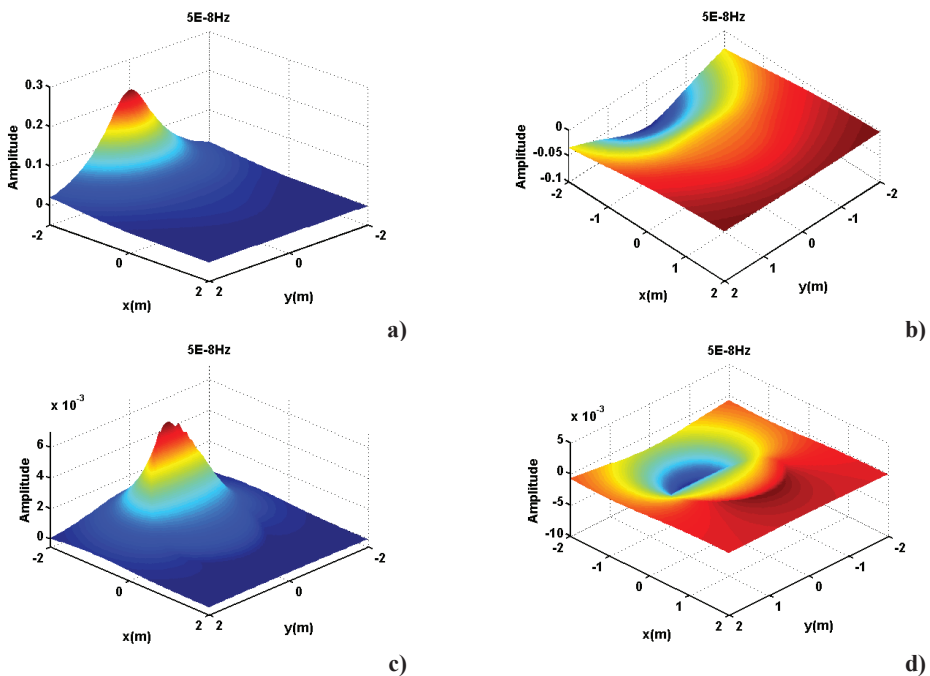


Figure 6: Verification and accuracy for frequency $5e^{-8}$ Hz: a) Real part of the analytical response; b) Imaginary part of the analytical response; c) Numerical error of the real part of the response using $r=0.2m$; d) Numerical error of the imaginary part of the response using $r=0.2m$.

3.2 Evaluation of average relative error

The average relative error was computed to better define the radius of the support domain and the number of nodal points that should be used to achieve more accurate results. The geometry of the problem described above was used to verify and study the behavior of the proposed model. The same grid of 6561 receivers was used. The difference between the analytical and the numerical response is computed at each receiver. To assess the global quality of the solution, the following average relative error is established

$$\bar{E} = \frac{1}{N_{rec}} \sum_{i=1}^{N_{rec}} \frac{|T(\mathbf{x}_i) - \hat{T}(\mathbf{x}_i)|}{|T(\mathbf{x}_i)|} \quad (29)$$

where N_{rec} is the total number of receivers, $T(\mathbf{x}_i)$ is the analytical solution and $\hat{T}(\mathbf{x}_i)$ is the numerical result.

The number of nodes on the boundary varies from 50 to 210 (Fig. 7). Internal nodes are uniformly distributed within the circular heterogeneous region and their number is defined such that the distance between them is similar as that between boundary nodes.

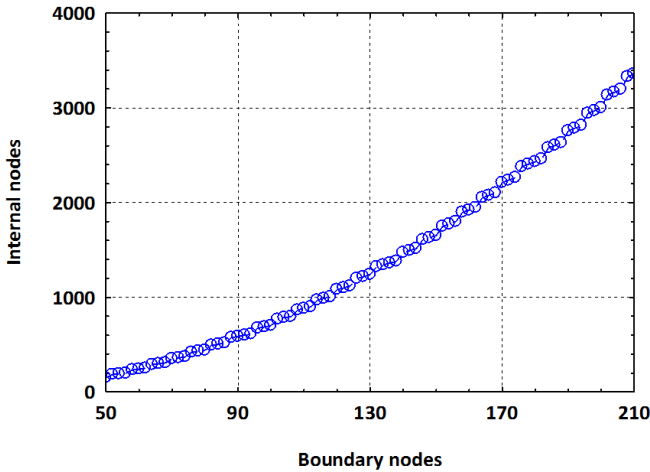


Figure 7: Number of boundary and internal nodes

The radius of the circular support domain is assumed to change from $r = 0.05$ m and $r = 0.5$ m, with an increment of 0.01 m. Four frequencies were analyzed, namely 0.0 Hz, $5.0e^{-8}$ Hz, $5.0e^{-7}$ Hz and $5.0e^{-6}$ Hz.

Figure 8 illustrates the average relative error. A log scale was used to better show the results. Note that responses are not computed when the radius of the circular support domain is not large enough to cover a sufficient number of nodes in the domain of definition to ensure the regularity of the matrix A.

As expected, it can be seen for the four frequencies analyzed that more nodal points are required as the frequency of excitation increases. It can also be observed that the average relative error reaches very low values at lower frequencies. The response becomes less exact for higher frequencies, but it is accurate enough to be considered a good result. A better result would require the use of more nodal points.

It can also be seen that the accuracy depends strongly on the radius of the circular support domain. This dependence is more relevant for high frequencies since the quality of the response changes markedly with the variation of radius of the circular support domain. As the frequency increases the best results are obtained for smaller radii of the circular support domain.

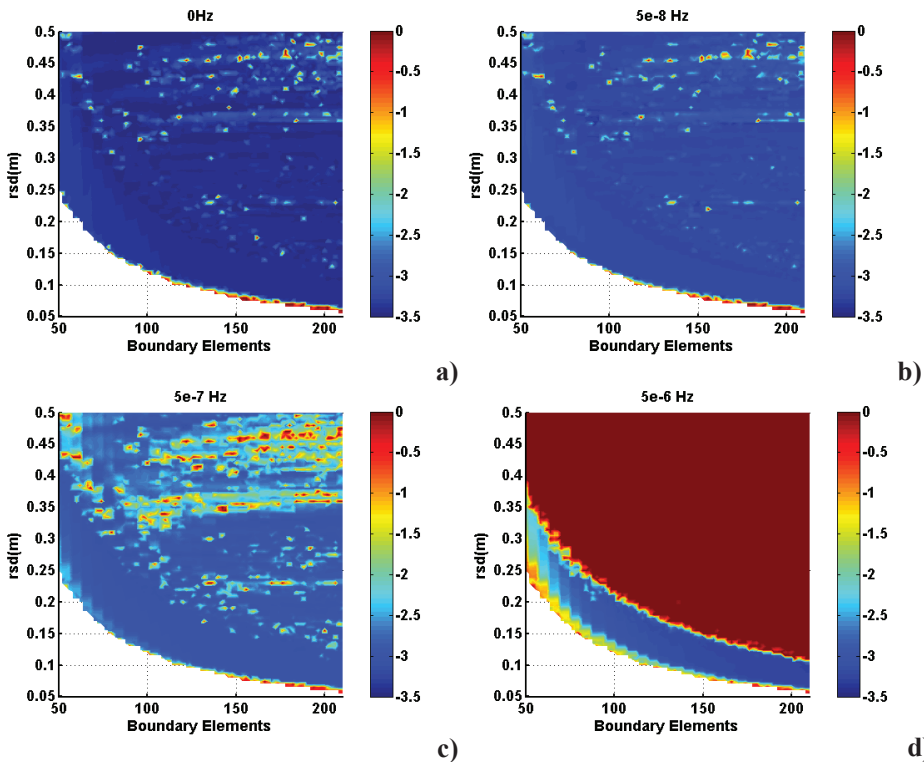


Figure 8: Average relative error, presented on a log scale, for the analytical solution: a) 0.0 Hz; b) $5e^{-8}$ Hz; c) $5e^{-7}$ Hz; d) $5e^{-6}$ Hz

4 Numerical example

The proposed model was used to simulate an infinite medium, Ω_3 , with known properties ($\rho_3 = 1860 \text{ kg.m}^{-3}$, $c_3 = 780 \text{ J.kg}^{-1}.\text{°C}^{-1}$ and $\lambda_3 = 0.72 \text{ W.m}^{-1}.\text{°C}^{-1}$), containing two localized regions, Ω_1 and Ω_2 , with radii of 1 m, where a variation of the thermal conductivity λ and the specific heat c occurs (see Fig. 9). The system was subjected to an external point heat source, T_{inc} , placed at $(-1.5 \text{ m}, -2.5 \text{ m})$.

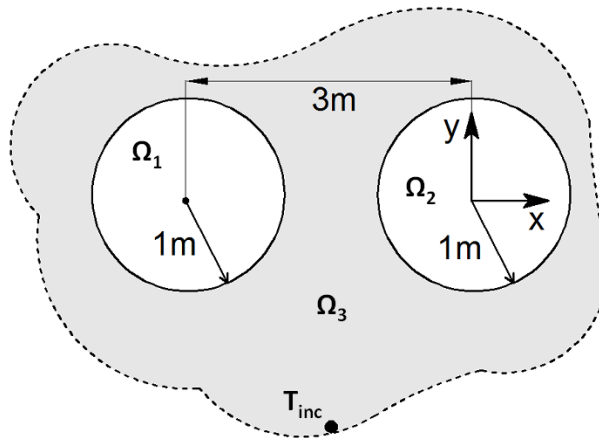


Figure 9: Geometry used in the numerical applications

Two cases were simulated, assuming different variations for conductivity and specific heat, as illustrated in Fig. 10. The value of density, ρ_3 was considered to be constant for the entire domain. For each case, the thermal conductivity and the specific heat variations within the circular non-homogeneous regions are assumed to occur in the radial direction and can be spatially represented by the following equations:

Thermal property variations in Case 1:

$$\begin{aligned}
 \lambda_1(\mathbf{x}) &= 0.72 \left[1 - 0.4305 \left[1.0 + \sin \left(\pi \sqrt{x^2 + y^2} + \frac{\pi}{2} \right) \right] \right] \\
 c_1(\mathbf{x}) &= 780 \left[1.25 - \frac{\sqrt{x^2 + y^2}}{4} \right] \\
 \rho_1 &= 1860 \text{ kg.m}^{-3}
 \end{aligned}
 \tag{30}$$

$$\begin{aligned}\lambda_2(\mathbf{x}) &= 0.72 \left[1 + 0.888 \left[1.0 + \sin \left(\pi \sqrt{x^2 + y^2} + \frac{\pi}{2} \right) \right] \right] \\ c_2(\mathbf{x}) &= 780 \left[1.25 - \frac{\sqrt{x^2 + y^2}}{4} \right] \\ \rho_2 &= 1860 \text{ kg.m}^{-3}\end{aligned}\quad (31)$$

Thermal property variations in Case 2:

$$\begin{aligned}\lambda_1(\mathbf{x}) &= 0.72 \left[1 - 0.49 \left[1.0 + \sin \left(\pi \sqrt{x^2 + y^2} + \frac{\pi}{2} \right) \right] \right] \\ c_1(\mathbf{x}) &= 780 \left[1.5 - \frac{\sqrt{x^2 + y^2}}{2} \right] \\ \rho_1 &= 1860 \text{ kg.m}^{-3}\end{aligned}\quad (32)$$

$$\begin{aligned}\lambda_2(\mathbf{x}) &= 0.72 \left[1 + 693.94 \left[1.0 + \sin \left(\pi \sqrt{x^2 + y^2} + \frac{\pi}{2} \right) \right] \right] \\ c_2(\mathbf{x}) &= 780 \left[1.5 - \frac{\sqrt{x^2 + y^2}}{2} \right] \\ \rho_2 &= 1860 \text{ kg.m}^{-3}\end{aligned}\quad (33)$$

The temperature field distribution was computed over a fine rectangular grid of 9211 receivers placed at $-5\text{m} \leq x \leq 2\text{m}$ and $-2\text{m} \leq y \leq 2\text{m}$. For each frequency, the discretization of the boundary of each heterogeneity made use of 200 boundary elements. The number of internal node points was defined such that the distance between neighboring internal points was similar to that between boundary nodes. These internal nodal points were distributed evenly across each circular non-homogeneous region.

Time responses are obtained by means of an inverse Fourier transform in the frequency domain. In order to prevent the aliasing phenomena, complex frequencies, with a small imaginary part of the form $\omega c = \omega - i\eta$ (with $\eta = 0.7\Delta\omega$, and $\Delta\omega$ being the frequency step), are used in the computation procedure. The constant η cannot be made arbitrarily large, since this leads either to a severe loss of numerical accuracy, or to underflows and overflows in the evaluation of the exponential windows.

The time evolution of the heat source amplitude can be diversified. The time Fourier transform of the incident heat field defines the frequency domain where the BEM solution needs to be computed $\hat{T}_0(x, y, \omega) = \int_0^\infty T_0(x, y, t) e^{-i\omega t} dt$. The response needs to be computed from 0.0 Hz up to very high frequencies. An intrinsic characteristic of this problem is that the heat responses decay very fast as the frequency increases, which allows us to limit the upper frequency for the solution.

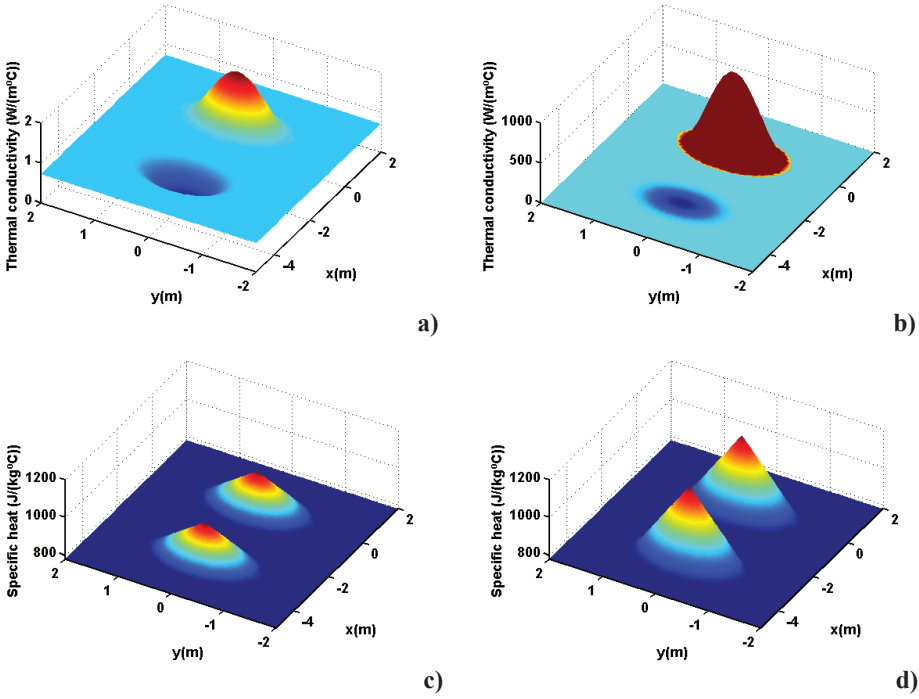


Figure 10: Numerical application: thermal property distribution: a) Thermal conductivity distribution in case 1; b) Thermal conductivity distribution in case 2; c) Specific heat distribution in case 1; d) Specific heat distribution in case 2

The final equation is given by

$$T(x, y, t) = \frac{1}{2\pi} \int_0^\infty \hat{T}_0(x, y, \omega) \hat{T}(x, y, \omega) e^{i\omega t} d\omega \tag{34}$$

which is computed as a discrete inverse fast Fourier transform.

The calculations were performed in the frequency range $[0.0, 1.975 \times 10^{-3}]$ Hz with a frequency increment of $\Delta f = 9.645061728 \times 10^{-7}$ Hz, which results in a time window of $1/(9.645061728 \times 10^{-7})$ s. The source starts emitting energy at instant $t = 4$ h and continues for 10h. The heat source time dependence is assumed to be rectangular, defined so that a maximum temperature increase of 20°C is recorded by the receiver located at $(-1.5 \text{ m}, -2.0 \text{ m})$.

A set of snapshots of the time domain simulations is presented to illustrate the resulting heat conduction across the geometrical model. Fig.11 shows the temperature field distribution at different time instants ($t = 30$ h, $t = 45$ h, $t = 60$ h and

$t = 72\text{h}$). At each instant two plots are displayed for each of the 2 cases. A color scale is used in the plots, with the red and blue shades corresponding respectively to higher and lower temperature amplitudes.

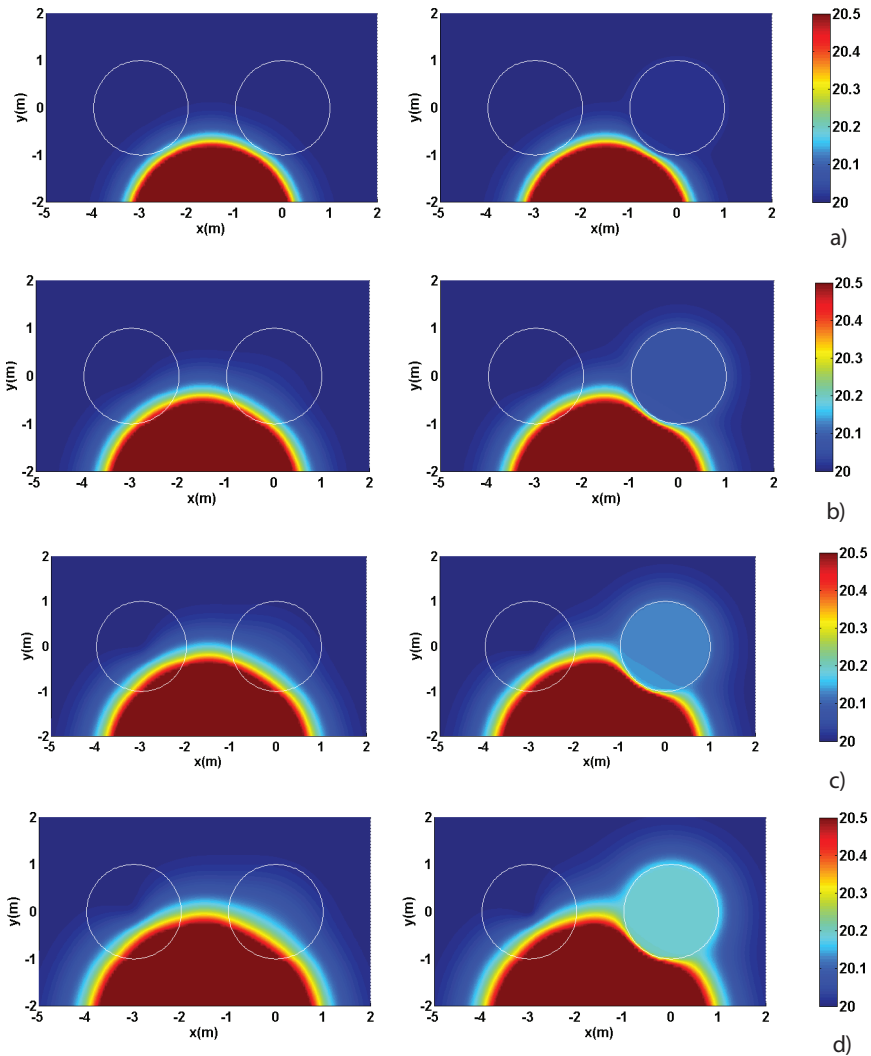


Figure 11: Numerical application - Temperature distribution (in °C) in the geometrical model: a) Time domain snapshots at $t=30\text{h}$; b) Time domain snapshots at $t=45\text{h}$; c) Time domain snapshots at $t=60\text{h}$; d) Time domain snapshots at $t=72\text{h}$

In the first plot, at $t = 30$ h (Fig. 11 a), for both cases, a small part of the incident temperature field has already reached the non-homogeneous parts of the medium. It can be observed that, in the circular region where the thermal conductivity has increased most, in case 2 the heat begins to spread more rapidly than in the other region, where the thermal conductivity falls to a very low value. This difference becomes more pronounced over time (Fig. 11 b to 11 d). But in case 1 this behavior is not yet discernible, since the conductivity variation in the non-homogeneous circular regions is less pronounced. At instants $t = 60$ h and $t = 72$ h (Fig. 11c) and (Fig. 11d), respectively) it can be seen that the low values of thermal conductivity act as a barrier to the heat flux and the process of heat dissipation is significantly slower than in the other two cases, where thermal conductivity increases. As expected, this behavior is more evident for the media with more pronounced conductivity variations, illustrated in case 2 (right plot).

For the same problem, the temperature response was analyzed at four receivers, over a time window of 288 h. The receivers' locations are illustrated in Fig. 12.

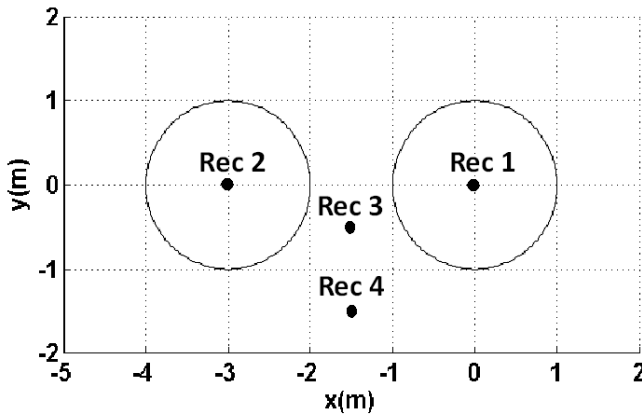


Figure 12: Numerical application

Fig. 13 a) and Fig. 13 b) show the variation of the temperature response over time at the receivers for cases 1 and 2, respectively. As expected, it can be observed that the response is higher at receiver 4, since it is nearest to the heat source. On the other hand, even though Rec 1 and Rec 2 are the same distance from the heat source, the temperature response reaches higher values at Rec 1 where the thermal conductivity values are significantly higher. This difference is clearer for the media with more pronounced conductivity variations, represented in case 2.

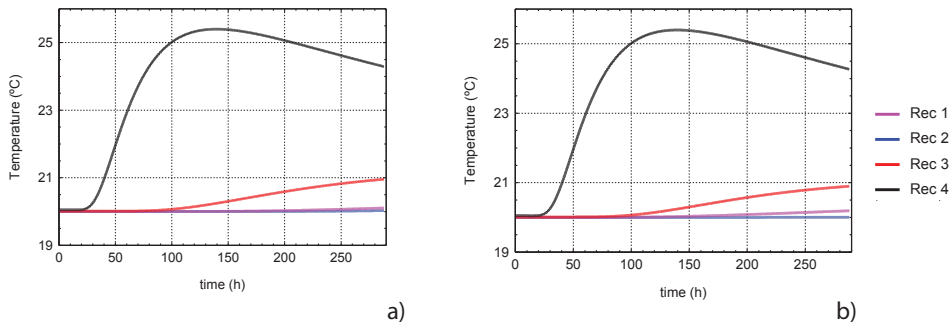


Figure 13: Numerical application: Temperature responses in time domain at four different receivers. a) Case 1; b) Case 2

5 Conclusions

A coupled numerical model using the meshless local Petrov-Galerkin (MLPG) method and the Boundary Element Method (BEM) has been proposed for the simulation of transient heat diffusion, in the frequency domain, of homogenous unbounded media containing localized regions within which the medium properties may vary. The BEM was used to simulate the heat propagation in the outer medium, while the MLPG was used to model the localized regions for which the BEM is not suitable.

The proposed model was verified against an analytical solution developed for a circular confined subdomain, in which the thermal properties (conductivity and specific heat) vary in the radial direction. The results showed the accuracy of the proposed model.

The average relative error was computed to better define the radius of the support domain and the number of the nodal points that should be used. The results showed that the accuracy of the proposed model depends on the number of nodal points and on the radius of the circular support domains. The higher the frequency of excitation the greater the number of nodal points required, and the best results are obtained for smaller radii of the circular support domains.

A numerical application was used to illustrate the applicability of the proposed model. The analysis of time domain temperature responses was found to be consistent with the physics of the problem.

Acknowledgements

This work has been supported by the University of Coimbra's Initiative Energy for Sustainability and by the Energy and Mobility for Sustainable Regions - EMSURE - Project (CENTRO-07-0224-FEDER-002004). This work has also been supported by the financial support of APVV-0014-10 and APVV-0032-10 (Slovak Research and Development Agency).

References

- Abreu, A. I.; Canelas, A.; Mansur, W. J.** (2013): A CQM-based BEM for transient heat conduction problems in homogenous materials and FGMs. *Applied Mathematical Modelling*, vol. 37, pp. 776-792.
- Atluri, S. N.** (2004): *The Meshless Local Petrov-Galerkin (MLPG) Method*. Tech. Science Press.
- Atluri, S. N.; Shen, S.** (2002): The Meshless Local Petrov-Galerkin (MLPG) Method: A Simple & Less-costly Alternative to the Finite Element and Boundary Element Methods. *CMES: Computer Modeling in Engineering & Sciences*, vol. 3, no.1, pp. 11-51.
- Atluri, S. N.; Sladek, J.; Sladek, V.; Zhu, T.** (2000): The local boundary integral equation (LBIE) and its meshless implementation for linear elasticity. *Computational Mechanics*, vol. 25, pp. 180-198.
- Atluri, S. N.; Zhu, T.** (1998): A new meshless local Petrov-Galerkin (MLPG) approach in computational mechanics. *Computational Mechanics*, vol. 22, pp. 17-27.
- Avila, R.; Atluri, S. N.** (2009): Numerical Solution of Non-steady Flows, Around Surfaces in Spatially and Temporally Arbitrary Motions, by using the MLPG method. *CMES: Computer Modeling in Engineering & Sciences*, vol. 54, no. 1, pp. 15-64.
- Bathe, K. J.** (1976): *Numerical Methods in Finite Element Analysis*. Prentice-Hall, New Jersey.
- Belytschko, T.; Organ, D.; Krongauz, Y.** (1995): Coupled finite element – element-free Galerkin method. *Comput. Mech.*, vol. 17, pp. 186 – 195.
- Brebbia, C. A., Telles, J. C.; Wrobel, L. C.** (1984): *Boundary Elements Techniques: Theory and Applications in Engineering*. Springer-Verlag, Berlin-New York.
- Cai, Z.; Mandel, J.; McCormick, S.** (1991): The finite volume element method for diffusion equations on general triangulations. *SIAM Journal on Numerical Analysis*, vol. 28, pp. 392-403.

Carslaw, H. S.; Jaeger, J. C. (1959): *Conduction of Heat in Solids*. Oxford University Press, Vivian Ridler, Walton Street, Oxford, second edition.

Chen, T.; Raju, I. S. (2003): A coupled finite element and meshless local Petrov-Galerkin method for two-dimensional potential problems. *Computer Methods in Applied Mechanics and Engineering*, vol. 192, pp. 4533 – 4550.

Cheng, R. J.; Liew, K. M. (2009): The reproducing kernel particle method for two-dimensional unsteady conduction problems. *Computational Mechanics*, vol. 45, pp. 1-10.

Ching, H. K.; Batra, R. C. (2001): Determination of Crack Tip Fields in Linear Elastostatics by the Meshless Local Petrov-Galerkin (MLPG) Method. *Computer Modeling in Engineering & Sciences*, vol. 2, no. 2, pp. 273-289.

Dai, B.; Zheng, B.; Liang, Q.; Wang, L. (2013): Numerical solution of transient heat conduction problems using improved meshless local Petrov-Galerkin method. *Applied Mathematics and Computation*, vol. 219, pp. 10044-10052.

Dong, L.; Atluri, S. N. (2012): Development of 3D Trefftz Voronoi Cells with Ellipsoidal Voids &/or Elastic/Rigid Inclusions for Micromechanical Modeling of Heterogeneous Materials. *CMC: Computers Materials and Continua*, vol. 30, no.1, pp. 39-82.

Dong, L.; Atluri, S. N. (2013): SGBEM Voronoi Cells (SVCs), with Embedded Arbitrary-Shaped Inclusions, Voids, and/or Cracks, for Micromechanical Modeling of Heterogeneous Materials. *CMC: Computers, Materials & Continua*, vol. 33, no.2, pp. 111-154.

Fairweather, G.; Karageorghis, A. (1998): The method of fundamental solutions for elliptic boundary value problems. *Advances in Computational Mathematics*, vol. 9, pp. 69–95.

Fairweather, G.; Karageorghis, A.; Martin, P. A. (2003): The method of fundamental solutions for scattering and radiation problems. *Engineering Analysis with Boundary Elements*, vol. 27, pp. 759–769, DOI: 10.1016/S0955-7997(03)00017-1.

Godinho, L.; Tadeu, A. (2012): Acoustic analysis of heterogeneous domains coupling the BEM with Kansa's method. *Eng. Anal. Bound. Elem.*, vol. 36, pp.1014-1026.

Godinho, L.; Tadeu, A.; Simões, N. (2006): *Accuracy of the MFS and BEM on the analysis of acoustic wave propagation and heat conduction problems*. In *Advances in Meshless Methods*, Jan S, Vladimir S (eds). Tech Science Press.

Gu, Y. T.; Liu, G. R. (2005): Meshless Methods Coupled with Other Numerical Methods. *Tsinghua Science & Technology*, vol. 10, pp. 8–10.

Han, Z. D.; Liu, H. T.; Rajendran, A. M.; Atluri, S. N.(2006): The Applications

of Meshless Local Petrov Galerkin (MLPG) Approaches in High-Speed Impact, Penetration and Perforation Problems. *CMES: Computer Modeling in Engineering & Sciences*, vol. 14, no. 2, pp. 119-128.

Hegen, D. (1996): Element-free Galerkin methods in combination with finite element approaches. *Comput. Methods Appl. Mech. Engrg*, vol. 135, pp. 143 – 166.

Juncu, Gh. (2008): Unsteady conjugate forced convection heat/mass transfer from a finite flat plate. *International Journal of Thermal Sciences*, vol. 47, pp. 972–984.

Karutz, H.; Chudoba, R.; Kratzig, W. B. (2002): Automatic adaptive generation of a coupled finite element/element-free Galerkin discretization. *Finite Elements in Analysis and Design*, vol. 38, pp. 1075-1091.

Li, Q. H.; Chen, S. S.; Kou, G. X. (2011): Transient heat conduction analysis using the MLPG method and modified precise time step integration method. *Journal of computational Physics*, vol. 230, pp. 2736-2750.

Li, Y. S.; Feng, W. J.; Xu, Z. H. (2009): Fracture analysis of cracked 2D planar and axisymmetric problems of magneto-electro-elastic materials by the MLPG coupled with FEM. *Computer Methods in Applied Mechanics and Engineering*, vol. 198, no. 30-32, pp. 2347–2359.

Lin, H.; Atluri, S. N. (2001): The Meshless Local Petrov-Galerkin (MLPG) Method for Solving Incompressible Navier-Stokes Equation. *CMES: Computer Modeling in Engineering & Sciences*, vol. 2, pp. 117-142.

Liu, G. R.; Gu, Y. T. (2000): Meshless local Petrov-Galerkin (MLPG) method in combination with finite element and boundary element approaches. *Computational Mechanics*, vol. 26, pp. 536-546.

Liu, G. R.; Gu, Y. T. (2000): Coupling of element free Galerkin and hybrid boundary element methods using modified variational formulation. *Comput. Mech*, vol. 26, pp. 166 – 173.

Mirzaei, D.; Dehghan, M. (2011): MLPG method for transient heat conduction problem with MLS as trial approximation in both time and space domains. *CMES: Computer Modeling in Engineering & Sciences*, vol. 72, no. 3, pp. 185-210.

Ochiai, Y. (2001): Steady heat conduction analysis in orthotropic bodies by triple-reciprocity BEM. *Computer Modeling in Engineering and Sciences*, vol. 2, no.4, pp. 435–446.

Ozisk, M. N. (1994): *Finite Difference Methods in Heat Transfer*. CRC Press Inc, USA.

Sellountos, E. J.; Vavourakis, V.; Polyzos, D. (2005): A new singular/hypersingular MLPG (LBIE) method for 2D elastostatics. *CMES: Computer Modeling in Engi-*

neering & Sciences, vol. 7, pp. 35-48.

Shirzadi, A.; Sladek V.; Sladek J. (2013): A local integral equation formulation to solve coupled nonlinear reaction- diffusion equations by using moving least square approximation. *Engineering Analysis with Boundary Elements*, vol. 37, pp. 8-14.

Singh, I. V.; Tanaka, M. (2006): Heat transfer analysis of composite slabs using meshless element free Galerkin method. *Computational Mechanics*, vol. 38, pp. 521-532.

Sladek, J.; Sladek, V.; Atluri, S. N. (2004): Meshless Local Petrov-Galerkin Method for Heat Conduction Problem in an Anisotropic Medium. *CMES: Computer Modeling in Engineering & Sciences*, vol. 6, no. 3, pp. 309-318.

Sladek, J.; Sladek, V.; Hellmich, Ch.; Eberhardsteiner, J. (2007): Heat conduction analysis of 3-D axisymmetric and anisotropic FGM bodies by meshless local Petrov-Galerkin method. *Computational Mechanics*, vol. 39, no. 3, pp. 323-333.

Sladek, J.; Sladek, V.; Hon, Y.C. (2006): Inverse heat conduction problems by meshless local Petrov-Galerkin method. *Eng. Anal. Bound. Elem.*, vol. 30, pp. 650-661.

Sladek, J.; Sladek, V.; Krivacek, J.; Zhang, Ch. (2003): Local BIEM for transient heat conduction analysis in 3-D axisymmetric functionally graded solids. *Comput. Mech.*, vol. 32, pp. 169-176.

Sladek, J.; Sladek, V.; Krivacek, J.; Zhang, Ch. (2005): Meshless Local Petrov-Galerkin Method for Stress and Crack Analysis in 3-D Axisymmetric FGM Bodies. *CMES: Computer Modeling in Engineering & Sciences*, vol. 8, no. 3, pp. 259-270.

Sladek, J.; Sladek, V.; Van Keer, R. (2003): Meshless local boundary integral equation method for 2D elastodynamic problems. *International Journal for Numerical Methods in Engineering*, vol. 57, pp. 235-249.

Sladek, J.; Sladek, V.; Wen, P.; Hon B. (2012): Inverse heat conduction problems in three-dimensional anisotropic functionally graded solids. *Journal of Engineering Mathematics*, vol. 75, no. 1, pp. 157-171.

Sladek, J.; Sladek, V.; Wen, P.H.; Aliabadi, M.H. (2006): Meshless Local Petrov-Galerkin (MLPG) Method for Shear Deformable Shells Analysis. *CMES: Computer Modeling in Engineering & Sciences*, vol. 13, no. 2, pp. 103-117.

Sladek, J.; Sladek, V.; Wen, P.H.; Hon, Y.C. (2009): The Inverse Problem of Determining Heat Transfer Coefficients by the Meshless Local Petrov-Galerkin Method. *CMES: Computer Modeling in Engineering & Sciences*, vol. 48, pp. 191-218.

Sladek, J.; Sladek, V.; Zhang, Ch. (2003): Transient heat conduction analysis in functionally graded materials by the meshless local boundary integral equation

method. *Comput. Material Science*, vol. 28, pp. 494-504.

Sladek, J.; Sladek, V.; Zhang, Ch.; Garcia-Sanchez, F.; Wunsche, M. (2006): Meshless Local Petrov-Galerkin Method for Plane Piezoelectricity. *CMC: Computers, Materials & Continua*, vol. 4, no. 2, pp. 109-117.

Sladek, J.; Stanak, P.; Han, Z. D.; Sladek, V.; Atluri, S. N. (2013): Applications of the MLPG Method in Engineering & Sciences: A Review. *CMES: Computer Modeling in Engineering & Sciences*, 92, No.5, 423-475.

Sladek, J.; Sladek, V.; Tan, C. L.; Atluri, S. N. (2008): Analysis of Heat Conduction in 3D Anisotropic Functionally Graded Solids, by the MLPG. *CMES: Computer Modeling in Engineering & Sciences*, vol. 32, no.3, pp. 161-174.

Sladek, V., Sladek, J.; Zhang, Ch. (2010): On increasing computational efficiency of local integral equation method combined with meshless implementations. *CMES – Computer Modeling in Engineering & Sciences*, vol. 63, pp. 243-263.

Sladek, V.; Sladek, J. (2010): Local integral equations implemented by MLS-approximation and analytical integrations. *Engineering Analysis with Boundary Elements*, vol. 34, pp. 904-913.

Sladek, V.; Sladek J.; Sator L. (2013): Physical decomposition of thin plate bending problems and their solution by mesh-free methods. *Engineering Analysis with Boundary Elements*, vol. 37, pp. 348–365.

Sladek, V.; Sladek, J.; Tanaka, M.; Zhang, Ch. (2005): Transient heat conduction in anisotropic and functionally graded media by local integral equations. *Engineering Analysis with Boundary Elements*, vol. 29, pp. 1047-1065.

Sladek, V.; Sladek, J.; Zhang, Ch. (2008): Local integral equation formulation for axially symmetric problems involving elastic FGM. *Engineering Analysis with Boundary Elements*, vol. 32, pp. 1012-1024.

Smyrlis, Y. S. (2006): The method of fundamental solutions: a weighted least squares approach. *Biosystems and Information Technology*, vol. 46, pp. 163–194.

Soares, D. Jr. (2009): An Iterative Time-Domain Algorithm for Acoustic-Elastodynamic Coupled Analysis Considering Meshless Local Petrov-Galerkin Formulations. *CMES: Computer Modeling in Engineering & Sciences*, vol. 54, no. 2, pp. 201-222;

Soares, D. Jr.; Sladek, V.; Sladek, J. (2012): Modified meshless local Petrov-Galerkin formulations for elastodynamics. *International Journal for Numerical Methods in Engineering*, vol. 90, no. 12, pp. 1508-1528.

Soric, J.; Li, Q.; Jarak, T.; Atluri, S. N. (2004): Meshless Local Petrov-Galerkin (MLPG) Formulation for Analysis of Thick Plates. *CMES: Computer Modeling in Engineering & Sciences*, vol. 6, no. 4, pp. 349-357.

Tadeu, A.; Prata, J.; Simões, N. (2012): Closed form integration of singular and

hypersingular integrals in 3D BEM formulations for heat conduction. *Mathematical Problems in Engineering*, vol. 2012, Article ID 647038, doi:10.1155/2012/647038.

Tadeu, A.; Simões, N.; Simões, I. (2010): Coupling BEM/TBEM and MFS for the simulation of transient conduction heat transfer. *Int J Numer Methods Eng*, vol. 84, no. 2, pp. 179–213.

Techapirom, T.; Luadsong, A. (2013): *The MLPG with improved weight function for two-dimensional heat equation with non-local boundary condition*. Journal of King Saud University – Science.

Vavourakis, V.; Polyzos, D. (2007): A MLPG4 (LBIE) Formulation in Elastostatics. *CMC: Computers, Materials & Continua*, vol. 5, no. 3, pp. 185-196.

Wu, X. H.; Tao, W. Q. (2008): Meshless method based on the local weak-forms for steady state heat conduction problems. *International Journal of Heat and Mass Transfer*, vol. 51, pp. 3103–3112.

Zan, Zhang, K.M.; Cheng, L.Y. (2008): Coupling of the improved element-free Galerkin and boundary element methods for two-dimensional elasticity problems. *Engineering Analysis with Boundary Elements*, vol. 32, pp. 100 – 107.

Zhang, X.; Zhang, P.; Zhang, L. (2013): An improved meshless method with almost interpolation property for isotropic heat conduction problems. *Engineering Analysis with Boundary Elements*, vol. 37, pp. 850 – 859.

Zhao, M.; Nie, Y. (2008): A Study of Boundary Conditions in the Meshless Local Petrov-Galerkin (MLPG) Method for Electromagnetic Field Computations. *CMES: Computer Modeling in Engineering & Sciences*, Vol. 37, No. 2, pp. 97-112.